PHOTONICS Research

Acousto-optic tunable ultrafast laser with vector-mode-coupling-induced polarization conversion

Yujia Li,[1] Ligang Huang,[1,*] Haonan Han,[1] Lei Gao,[1] Yulong Cao,[1] Yuan Gong,[2] Wending Zhang,[3] Feng Gao,[4] Iroegbu Paul Ikechukwu,[1] and Tao Zhu[1,5]

[1]Key Laboratory of Optoelectronic Technology & Systems, Ministry of Education, Chongqing University, Chongqing 400044, China
[2]Key Laboratory of Optical Fiber Sensing and Communications, Ministry of Education, University of Electronic Science and Technology of China, Chengdu 611731, China
[3]MOE Key Laboratory of Material Physics and Chemistry under Extraordinary Conditions and Shaanxi Key Laboratory of Optical Information Technology, School of Science, Northwestern Polytechnical University, Xi'an 710072, China
[4]MOE Key Laboratory of Weak-Light Nonlinear Photonics, TEDA Applied Physics Institute and School of Physics, Nankai University, Tianjin 300457, China
[5]e-mail: zhutao@cqu.edu.cn
*Corresponding author: lghuang@cqu.edu.cn

Received 6 March 2019; revised 30 April 2019; accepted 13 May 2019; posted 14 May 2019 (Doc. ID 361696); published 24 June 2019

Acousto-optic interactions, employed in the ultrafast laser regulation, possess remarkable advantages for fast tuning performance in a wide spectral range. Here, we propose an ultrafast fiber laser whose wideband tunability is provided by an acousto-optic structure fabricated with an etched single-mode fiber. Because of the laser polarization conversion induced by the coupling between the core and cladding vector modes in the etched fiber, a band-pass characteristic of the acousto-optic interaction is achieved to effectively regulate the inner-cavity gain range. Cooperating with a saturable absorber based on single-wall carbon nanotubes (SWCNTs) with polarization robustness, a soliton operating state is achieved in the tunable erbium-doped fiber laser. By controlling the acoustical wave frequency from 1.039 to 1.069 MHz, this soliton laser can be conveniently tuned in a wide spectral range from 1571.52 to 1539.26 nm. Meanwhile, the laser pulses have near-transform-limited durations stably maintaining less than 2 ps at different wavelength channels, owing to the broadband nonlinear absorption of SWCNTs.

https://doi.org/10.1364/PRJ.7.000798

1. INTRODUCTION

Novel ultrafast lasers with flexible wideband tunability have attracted tremendous research interest because of their widespread application fields, such as precision metrology, fast controlling of chemical reactions, high-speed optical communications, and nonlinear deep-tissue microscopy [1–5]. Currently, the birefringence filtering effect is one of the most widely used methods to tune fiber lasers operating with various soliton types [6–10]. However, output at different wavelength channels is achieved by carefully adjusting polarization controllers (PCs). It is very difficult to quantitatively calibrate the relationship between the wavelengths and states of PCs and simultaneously maintain a polarization consistency of different tuning channels, particularly in non-polarization-maintained fiber cavities. Thus, various tunable band-pass components, such as the tunable Fabry–Perot-based filter and the rifled aluminum diffraction grating, have been employed to successfully select the gain range of ultrafast laser cavities and achieve organized wavelength tunability [11–16]. To date, although state-of-the-art commercial bulk filters reach a tuning range of 100 nm with a bandwidth of over 10 nm, most of them still need to manually adjust passbands, assisted with internal mechanical stepping systems, which goes against a remote, fast, and automatic laser regulation. Various fiber gratings have been used for controlling of ultrafast fiber lasers, owing to their flexible wavelength tunability induced by the manageable effective refractive index. Among these, uniform and chirp fiber Bragg gratings allow wide enough gain profiles inside cavities to support the oscillation of solitons [17–20]. However, their narrow bandwidths and large dispersion seriously widen pulse durations. The thermal- and opto-fluidic-controlled long-period gratings with wide passbands and sensitive refractive index are mainly employed in slow lasing wavelength tuning [21,22].

Fortunately, acousto-optic fiber devices employed for tuning of ultrafast lasers are worth exploring because of their superior advantages, which include wideband tunability and

fast wavelength switching [23]. The switch response time of the acousto-optic interaction (AOI), which is determined by the transit time of the acoustic wave propagation in the AOI region, can reach several tens of microseconds [24,25]. In addition, the wavelength can be tuned without any adjustment of the mechanical setup inside the cavity. Currently, the main technical challenge of their cooperation with wide-band tunable ultrafast lasers is their inherent band-rejection spectral characteristics. Numerous efforts have been devoted to obtaining those devices with a band-pass property. Offset splicing and core mode blockers will increase insertion loss, which may render acoustically induced fiber gratings (AIFGs) incompatible with laser cavities [26,27]. Cladding coupling with fiber tapering requires complex fabrication, because careful adjustment of the coupling distance between taper and cladding is necessary [28]. Moreover, due to small sizes of the taper region, optical performance can be easily influenced by the external airflow and dust, which needs additional special packaging to ensure the operation stability of ultrafast laser systems. It is worth noting that vector mode coupling induced by AOIs has been experimentally demonstrated [29,30]. The polarization conversion caused by the coupling of vector modes can achieve excellent wavelength-selection performance, such as high stability, tolerable insertion loss, passbands wide enough for soliton generation, and lack of frequency shift, so they easily cooperate with ultrafast laser systems.

In this work, we build an acousto-optic tunable ultrafast laser mode locked by single-wall carbon nanotubes (SWCNTs) with insensitivity to polarization. Coupling between core and cladding vector modes is excited within the laser cavity by the acoustically induced transverse refractive index perturbations (RIPs) on the fiber cross section. Only the laser with resonant wavelengths of the AOI has a polarization rotation induced by the mode coupling. Hence, the resonant light can pass through the polarization analyzer with low loss, whereas the nonresonant light cannot. Thus, the lasing wavelength selected by the resonant condition can be acoustically controlled without the adjustment of polarization controllers. Because of the SWCNT's wideband saturable absorption and anomalous cavity dispersion, the laser operating in a conventional soliton state can be tuned in a wavelength range of over 32 nm with acoustical frequency changed from 1.039 to 1.069 MHz. The pulse duration remains less than 2 ps during the tuning process. Considering that acousto-optic structures attain wide and fast tunability with ease, it will benefit their applications in ultrafast laser systems.

2. PRINCIPLE

In a tunable ultrafast laser system, the effective gain range can be restricted by the AOI inside the cavity. For single-mode fiber (SMF), an acoustic flexural wave vibrates parallel to the fiber cross section and propagates longitudinally to generate a dynamic grating. An asymmetrical RIP is induced to the cross section, while a longitudinal periodic refractive index is generated. When the laser enters the AOI region, mode coupling between the core mode (LP_{01}) and cladding mode (LP_{11}) can be excited by the RIP. We define the x axis along the vibrational direction of the acoustical wave, whereas the y axis within the cross-section is vertical to the vibrational direction, and the z axis is along the fiber. LP_{01} and LP_{11} modes correspond to the vector mode groups $\{HE_{11x}, HE_{11y}\}$ and $\{TM_{01}, TE_{01}, HE_{21even/odd}\}$, respectively. The RIP can be expressed by $\Delta n = n_0(1+\chi)K^2 u_0 x$, where n_0 is the refractive index of the core, χ is the elasto-optical coefficient of silica, and K and u_0 are the wave vector and amplitude of the acoustical wave, respectively [31]. The coupling coefficient κ_{ab} is proportional to the overlap integral of the involved vector modes weighted with the perturbation Δn, which is expressed with the polar coordinate as [32]

$$\kappa_{ab} \propto \int_0^R \int_0^{2\pi} \overrightarrow{u_{01}^a} \cdot \overrightarrow{\Phi_{11}^b(\varphi)} F_{01}(r) F_{11}(r) r^2 \cos(\varphi) \mathrm{d}\varphi \mathrm{d}r, \tag{1}$$

where R is the cladding radius, φ is the angular variable with respect to the vibrational direction of the acoustical wave, and r is the radial variable with respect to the center of the cross section. a equals 1 and 2, corresponding to the vector core modes HE_{11x} and HE_{11y}, respectively. b equals 1, 2, 3, and 4, corresponding to vector cladding modes TM_{01}, TE_{01}, HE_{21even}, and HE_{21odd}, respectively. u_{01} and $\Phi_{11}(\varphi)$ are unit direction vectors of the vector mode groups LP_{01} and LP_{11}, respectively. $F_{l1}(r)(l = 0, 1)$ is the electric field radial distribution of the vector mode in the LP_{l1} group. According to the integral results ($\kappa_{12}, \kappa_{14}, \kappa_{21}, \kappa_{23} = 0$, while $\kappa_{11}, \kappa_{13}, \kappa_{22}, \kappa_{24} \neq 0$), HE_{11x}/HE_{11y} couples only to $\{TM_{01}, HE_{21even}\}/\{TE_{01}, HE_{21odd}\}$.

As seen as Fig. 1, the longitudinal index modulation period is determined by $t\Lambda = (\pi RC/f)^{1/2}$ [33], where C is defined as the speed of the acoustical wave in SiO_2, f is the driving signal frequency, and R is the radius of the fiber. We first consider the mode coupling between the core mode HE_{11y} and cladding mode TE_{01}. Provided the resonant condition $\lambda_{TE} = \Lambda\Delta n_{ab}(a = 2, b = 2)$ is satisfied, core mode HE_{11y} will couple to cladding mode TE_{01}. In the equation, λ_{TE} is the wavelength of the injected laser. Λ is the grating period, and Δn_{ab} is the effective refractive index difference between the involved core and cladding vector modes. If the over-coupling condition $\kappa_{22} L_A = \pi$ is satisfied, the energy will be completely coupled from TE_{01} back to HE_{11y}, while the polarization of HE_{11y} is rotated by 180°, resulting from the half-wave loss induced by the over-coupling process. Coupling to other vector cladding modes is similar. Because of the mode dispersion,

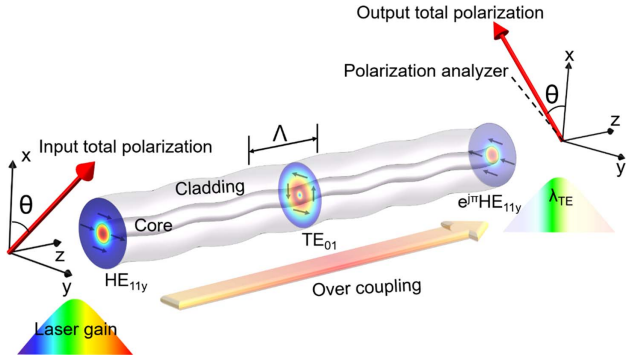

Fig. 1. Laser polarization conversions of core vector modes. Laser mode over-coupling process is induced by the AOI between the core vector mode HE_{11y} and cladding vector mode TE_{01}, and Λ is the grating period.

Δn_{11} is different from Δn_{22}, and scalar modes will split to the corresponding vector mode groups. However, Δn_{13} always equals Δn_{24}, because HE_{21odd} and HE_{21even} are strictly degenerated, if we ignore the inherent fiber birefringence. There are just three different phase matching conditions for TE_{01}, TM_{01}, and $HE_{21even/odd}$ under the same driving frequency, corresponding to wavelengths at λ_{TE}, λ_{TM}, and λ_{HE}, respectively.

The polarizer and analyzer (dashed line within the x–y plane) are perpendicularly located at the input and output ports of the AIFG, respectively, and θ is the angle between the vibration direction of the acoustical wave and the polarizer. The polarization state (the left red arrow within the x–y plane) of the injected laser is determined by the polarizer, which is projected to the x axis and y axis, corresponding to core modes HE_{11x} and HE_{11y}, respectively. Because of the phase matching condition, $\lambda_{TE/TM} = \Lambda\Delta n_{22/11}$, only the $HE_{11y/x}$ mode couples with TE_{01}/TM_{01} mode. The y/x polarization component will rotate 180° in the condition of over-coupling, while the x/y polarization component remains constant. Thus, the recombinant laser polarization is symmetrical to the input polarization with respect to the x/y axis, as shown as the left red arrow. According to the polarization projection law, the laser with wavelength at $\lambda_{TE/TM} = \Lambda\Delta n_{22/11}$ passes the polarization analyzer with a theoretical intensity transmission (dB), γ, which can be expressed by $\gamma(\theta) = 10\log_{10}[\sin^2(2\theta)]$. If θ equals 45°, the laser with wavelengths at λ_{TE} and λ_{TM} has a polarization rotation of 90°, and passes through the polarization analyzer theoretically without any loss. Light with wavelengths far from λ_{TE} and λ_{TM} within the gain range will be isolated by the polarizer and analyzer with perpendicular directions. Because of the mode dispersion features of the cladding-etched SMF with diameter larger than 20 μm, λ_{TE} is inherently smaller than λ_{TM}, which can be utilized as an important judgement of vector modes in accordance with the transmission spectrum. In general, by the polarization conversion of the core vector modes, the restriction of the laser gain is achieved, which can be tuned by changing the acoustic frequency. It is worth noting that coupling to HE_{21} theoretically cannot achieve polarization conversion with the circular symmetrical distribution of fiber refractive index. Because of the degeneration of HE_{21odd} and HE_{21even}, HE_{11x} and HE_{11y} will simultaneously couple to HE_{21odd} and HE_{21even}. Thus, the over-coupling process makes the total laser polarization rotate 180°, and the injected laser cannot pass the orthometric polarizer and analyzer. The over-coupling process makes the total laser polarization rotate 180°, even though the input light has both polarization components of HE_{11x} and HE_{11y}. Thus, the injected laser still cannot pass the orthogonal polarizer and analyzer at the resonant wavelength of λ_{HE}.

3. EXPERIMENTAL SETUP AND FABRICATION

The experimental system of the acousto-controlled tunable ultrafast laser is shown as Fig. 2. Different from other tunable laser systems [9], the wavelength selection and mode-locking mechanisms are divided in this cavity to avoid mutual disturbances between them. A commercial 980 nm semiconductor laser is used to provide the gain condition, which is connected with the 1 m erbium-doped fiber (EDF, Er80-8/125, LIEKKITM) by a 980/1550 wavelength division multiplexer (WDM). This all-fiber ring cavity consists mainly of SMF with a dispersion coefficient of 18 ps/(nm·km) and EDF with a dispersion coefficient of 15.7 ps/(nm·km) to ensure an anomalous net group velocity dispersion. Mode-locking performance is achieved by a saturable absorber (SA) fabricated with an SWCNT film. As in the previous discussion, the band-pass property depends on the polarization of the injected light in this cavity. Thus, to avoid influence on the mode-locking operation, we try to select an SA with low polarization sensitivity. SWCNT, as a type of low-dimensional material, has wideband nonlinear performance and polarization robustness, which benefits the mode-locking operation in this cavity [34–37]. The isolator placed behind the SA is used to determine the laser operation direction. A polarization controller (PC 3) is employed to adjust the laser polarization to match Polarizer 1 within the red box. Output and feedback of the laser cavity are achieved by an optical coupler (OC) with a coupling ratio of 1:9.

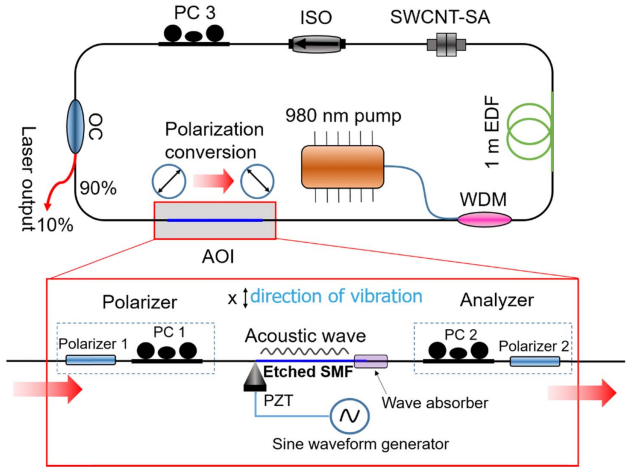

Fig. 2. Experimental setup of the tunable ultrafast fiber laser whose mode-locking property and tunability are achieved by an SWCNT-SA and AOI, respectively.

Here, in the quest to maintain the all-fiber structure of the laser cavity, we try to use components with SMF pigtails to achieve polarization conversion in the acousto-optic structure shown within the red box. Linear Polarizer 1 combined with PC 1 establishes a direction-adjustable polarizer. The generation of the band-pass property depends on the relative angle between the polarizer and analyzer. The adjustable polarization states of the injected and output light in the system are necessary. If we want to remove PC 1 and PC 2, we can use adjustable polarizers with SMF pigtails. We used standard SMF (Corning, 28e) as the acousto-optic medium. To enhance the acoustic flexural wave intensity in the fiber and enlarge the mode dispersion, the SMF's diameter is properly etched to ~30 μm in hydrofluoric acid, as seen in Fig. 3(a). Although the cladding diameter is changed, the etched fiber can still support only one core mode group, LP_{01}. The sine acoustic flexural wave is excited by an aluminum cone with a piezoelectric transducer (PZT) driven by a waveform generator (33120A, Agilent). The distance between the PZT's action point and

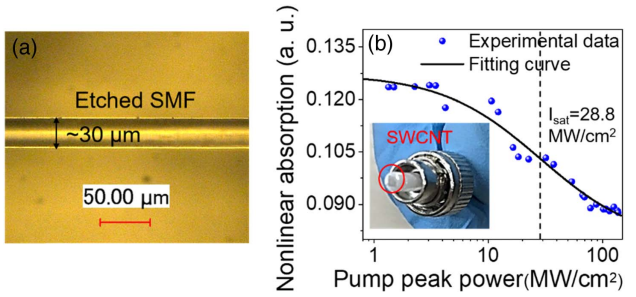

Fig. 3. (a) Photograph of the etched SMF with a diameter of 30 μm. (b) Absorptivity of the fiber-ferule SA with different pump peak intensities and the corresponding nonlinear fitting curve; the inset is the photograph of the SWCNT-SA. The SWCNT film is shown within the red circle.

the etched region is 0.5 cm, and ultraviolet curing adhesive is used to fix the action point on the lower surface of the cladding. The PZT's vibration direction along the x axis is perpendicular to the horizontal plane. We adjust the effective interaction length as ~13.5 cm by properly moving the position of an acoustical wave absorber (index matching liquid). Similarly, PC 2 and linear Polarizer 2 form a direction-adjustable polarization analyzer.

The SWCNT-SA used is prepared by intensively mixing aqueous polyvinyl alcohol and SWCNT dispersion liquid with a high-power blender. After dehydration, the mixture becomes a semitransparent gray film. As seen as the inset of Fig. 3(b), the SWCNT film is coated onto the clean end face of a fiber connector. This connector and another one without SWCNTs are inserted into a fiber flange, which provides SWCNTs with an enclosed environment. The nonlinear absorption characteristic of the SA is measured by the typical two-balanced detection method [38]. Figure 3(b) shows the SA's absorptivity under different pump peak intensities and the corresponding nonlinear fitting curve that can be expressed by the simplified two-level model:

$$\alpha(I) = \alpha_{\text{non}}/(1 + I/I_{\text{sat}}) + \alpha_l, \tag{2}$$

where $\alpha(I)$ is the intensity-dependent absorptivity, I_{sat} is the saturable intensity, I is the injected light intensity, α_l is the linear absorptivity, and α_{non} is defined as the nonlinear absorptivity. According to the fitting results, the modulation depth of the SA is ~4%.

4. RESULTS AND DISCUSSION

Considering the EDF used as the gain medium in this laser cavity, it is necessary first to confirm the tunable spectral characteristics of the induced AOI in the C-band. The band-pass property and tunability of the acousto-optic structure inside the red box, as shown in Fig. 2, are measured. A super-broadband light source is injected into Port 1, and the spectra are monitored from Port 2. Figure 4(a) shows the transmission spectra with different relative direction of the polarizer (Polarizer 1 and PC 1) and analyzer (Polarizer 2 and PC 2) with driving frequency of 1.052 MHz and driving power of 21.84 dBm. As mentioned in our previous discussion, if the polarizer

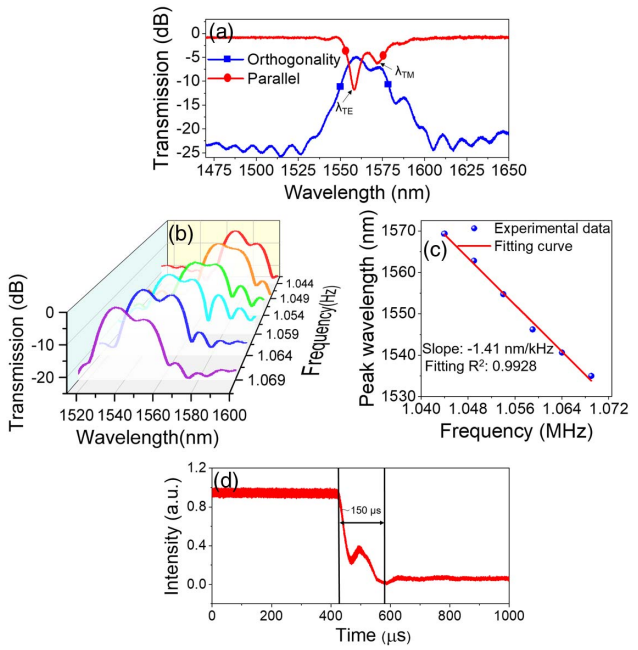

Fig. 4. Characterization of the tunable band-pass spectral property: (a) conversion of the transmission spectrum from band-injection to band-pass, corresponding to different relative polarization states of PCs 1 and 2; (b) transmission spectra of the AIFG with different driving signal frequencies; (c) corresponding peak wavelengths with different acoustic wave frequencies; (d) AOI wavelength-switch response time.

and analyzer are parallel, only the light with wavelengths selected by the phase matching condition will have a polarization rotation and be isolated by linear Polarizer 2. Because of the degeneration of two HE_{21} modes, two obvious loss peaks exist in the red dashed spectra, corresponding to λ_{TE} and λ_{TM}. When we adjust PC 2 to make the analyzer vertical to the polarizer, the spectrum is switched from the band-rejection to a band-pass shape, as seen as the blue solid line, and two transmission peaks have good correspondence to the loss peaks in the band-injection spectrum. A non-negligible loss still exists for the resonant wavelength. The resonant light can propagate through the analyzer without any loss only when the polarization directions of the analyzer and the output light from the etched fiber are aligned completely parallel. This is an ideal situation that is difficult to achieve, considering that the non-polarization-maintaining fiber devices are used in this cavity. In addition, the unavoidable scattering of the excited cladding mode in the etched fiber also causes some additional loss.

As in the previous discussion, θ equaling 45° is the ideal situation. The components used in this cavity are all fiber and non-polarization-maintaining. Thus, an acceptable insertion loss for the laser system still exists, mainly due to the unwanted direction deviation between polarizer and vibration of the PZT in actual operation. Moreover, the transmission loss of the cladding modes (TE_{01} and TM_{01}) in the etched fiber is unavoidable, resulting in a slight energy decrement during the over-coupling processes. It is worth noting that the transmission intensities at resonant wavelengths of λ_{TE} and λ_{TM} are

different. According to the wavelength selection induced by the polarization conversion, the transmission loss at the analyzer strongly depends on the polarization rotation degree. The difference of the conversion efficiencies of TE_{01} and TM_{01} mainly causes different polarization rotations of the core modes. This is a comprehensive consequence mainly induced by the unavoidable random fiber birefringence, inherent material dispersion, non-uniformity of the etched fiber diameter, and driving signal power. The reason for the continuous variation of the spectrum shape for different frequencies is mainly the different evolution situations of the polarization conversions of the light at wavelengths of λ_{TE} and λ_{TE}. Considering the wavelength interval of λ_{TE} and λ_{TM} (~15 nm) because of the degeneration of TE_{01} and TM_{01} modes and a wide tuning range of several-tens-of nanometers, it is very difficult to completely maintain an ideal over-coupling state of the TE resonance and TM resonance. The over-coupling to TE and TM modes will be differently influenced by the unintentional birefringence of the SMF, which will induce different additional phases to the y- and x-polarization components. Thus, it is normal to observe variations of the relative amplitudes when the driving frequency is changed. Quantitative analysis and control of the relative coupling intensity of TE_{01} and TM_{01} will be further studied in our future work. In this laser cavity, the bandwidth at λ_{TE} has already been wide enough to provide effective gain range for the oscillation of a mode-locked laser. As shown as Fig. 4(b), the transmission spectrum has a redshift by adjusting the driving frequency from 1.069 to 1.044 MHz, which is in agreement with the prospective tuning tendency because of the increased grating period. Figure 4(c) plots peak wavelengths under different driving frequencies and the corresponding fitting curve, indicating that the AOI approximately has a linear tunability within the C-band, which can be employed for organized lasing wavelength regulation.

Ultrafast laser systems can be different, but the excellent fast tuning mechanism should have a universality and portability. The inherent fast property of the tunable component and its compatibility with the ultrafast laser system are the preconditions of fast tuning. The upper limit of the lasing tuning speed should depend on the switch response of the AOI device. Therefore, we focus on the discussion of the AOI's response time. No matter what the specific AOI structure is, if the AOI is tuned to a new resonant wavelength, the acoustical wave with a new frequency has to completely cover the previous acoustical wave in the etched fiber. The response time can be simply estimated by the equation $t_{res} = L_{ao}/v_g$, where L_{ao} is the AOI length, the v_g equaling $2(\pi RCf)^{1/2}$ is the group velocity of acoustical wave in the etched fiber, and C equals 5760 m/s. If we assume the driving frequency of ~1 MHz, we can use the equation $t_{res} = L_{ao}/v_g$ to theoretically estimate the tuning response time of this device as ~130 μs. Thus, the AOI in our system can achieve a state switch time of the order of 100 μs between two filtering wavelengths. To confirm this fast wavelength-switch property, we make the signal laser's wavelength align with the left rising edge of the transmission spectrum of the AOI. The AOI's transmission spectrum is controlled by a driving signal with the frequency-shift keying mode (the driving frequency is hopping between two values), which causes a fast light intensity change. The normalized light intensity change is shown in Fig. 4(d), where the response time is about 150 μs. This value is influenced mainly by the etched fiber diameter, AOI length, and driving frequency.

By properly adjusting the PCs (1 and 2), the polarization direction of the polarizer can be approximately vertical to the analyzer and meanwhile parallel to the vibration direction of the acoustical wave. To decrease the cavity loss, PC 3 also has to be properly adjusted to enable the polarization of the inner-cavity laser match with Polarizer 1. If we turn off the waveform generator and set the 980 nm pump power as 110 mW, the orthogonality of the polarizer and analyzer will induce a large insertion loss to the cavity because of the sufficient polarization-dependent loss of Polarizers 1 and 2. Thus, this cavity cannot satisfy the gain threshold for a laser oscillation. Because the AIFG is located behind the OC, we can only observe a weak spontaneous emission spectrum, shown as the black dashed–dotted line in Fig. 5(a). When the acoustic flexural wave with a frequency of 1.049 MHz and a driving power of 18.35 dBm is added into the etched fiber with other devices fixed in this cavity, the laser can operate in a self-started mode-locking state with the pump power unchanged, as seen as the red solid line, because the band-pass property is generated. We can observe the symmetrical Kelly sidebands in the spectrum, demonstrating that the conventional soliton is generated due to the anomalous cavity dispersion. In this cavity, the mode-locking mechanism is completely due to the SWCNT-SA used. In contrast, this laser can operate in a continuous-wave state under this pump power level only when we remove this SA. The generated 3 dB spectral bandwidth of the mode-locked laser is 1.6 nm. Pulse trains and frequency spectra of the laser are measured by an oscilloscope (GA1102CAL, Gaatten) and a radio-frequency analyzer (DSA815, Rigol), respectively. The typical pulse property in the time domain of the output laser

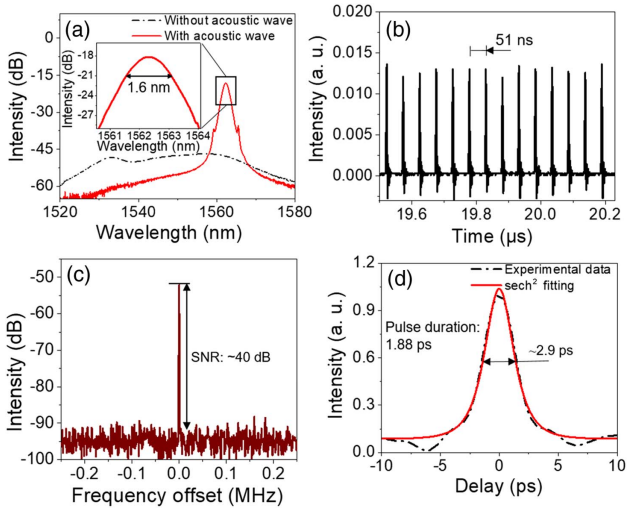

Fig. 5. Characterization of the soliton operation: (a) output spectra with and without the acoustic wave driving; inset is an enlargement of the local spectrum near the center wavelength; (b) pulse train in time domain; (c) radio-frequency spectrum of the fundamental frequency component; (d) autocorrelation trace and its $sech^2$ fitting curve.

is confirmed in Fig. 5(b), where the pulse period is 51 ns, corresponding to a repetition frequency of 19.6 MHz. As seen in Fig. 5(c), the signal-to-noise ratio (SNR) of the fundamental-frequency component reaches 40 dB, indicating good short-time stability, which is influenced mainly by the external temperature fluctuation and inherent fiber vibration within such a long cavity. As shown as Fig. 5(d), to estimate the pulse duration, the auto-correlation trace of laser pulses is well fitted by the sech^2 function, and the full width at half-maximum of the fitting curve is 2.9 ps, corresponding to a pulse duration of 1.88 ps. Thus, the time–bandwidth product (TBP) is calculated as merely ~0.37, a value that approaches the standard transform limit of 0.315, indicating that the pulse in this cavity is just slightly chirped.

Figure 6(a) compares the transmission spectrum (measured from Port 1 to Port 2) and the output spectrum of the mode-locked laser under the same driving frequency of 1.049 MHz. The overall loss (~11 dB) of the laser system consists mainly of the inherent insertion loss induced by these fiber devices (the OC with10% output coupling, the three PCs, the two polarizers, the isolator, the SA, the WDM, and the connection loss) and mode-coupling insertion loss of the etched fiber. The insertion loss of the etched fiber caused by the mode coupling can reach ~3 dB, which does not include the inherent insertion losses of Polarizers 1 and 2 and PCs 1 and 2. The total insertion loss induced by the structure inside the red box of Fig. 2 is ~6 dB, which does enlarge the laser oscillation and mode-locking thresholds. In this experiment, this insertion loss is still completely adaptable for soliton operation. As seen as the green shadow part, the peak wavelength of the laser is located within

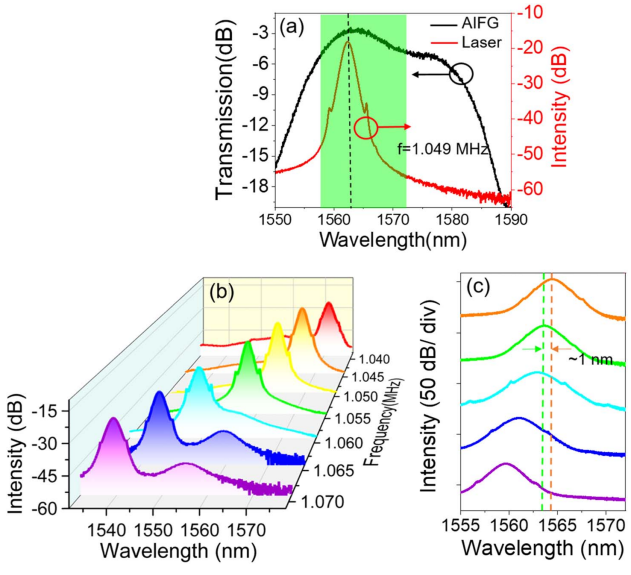

Fig. 6. Laser tuning test. (a) Transmission spectra of the AIFG and the output laser with the same driving frequency of 1.049 MHz, where the green shaded area represents the wavelength range within the 3 dB bandwidth of the transmission spectrum. (b) Spectral evolution with increment of the driving frequency from 1.039 to 1.069 MHz. (c) Spectral evolution with a smaller driving frequency interval of 1 kHz, where the two dashed lines are aligned with the corresponding color-coded laser spectra.

the 3 dB bandwidth of the transmission spectrum, and meanwhile the peak wavelength of the laser is close to the transmission peak of the TE_{01} mode. This phenomenon demonstrates that the oscillation and tunability of the laser are indeed dependent on the gain restriction induced by the AOI. However, the peak lasing wavelength cannot strictly align the peak transmission at all the tuning channels of this cavity, because the practical lasing peak wavelength is a certain result of complex mode competition under the inhomogeneous inner-cavity gain and transmission profiles induced by all the devices in this long laser cavity. It is normal for the peak lasing wavelength to slightly deviate from the transmission peak at some tuning channels, while the lasing peak wavelength is still kept within the 3 dB bandwidth of the transmission spectrum.

As seen in Fig. 6(b), when we change the driving frequency from 1.039 to 1.069 MHz, the lasing peak wavelength can be acoustically tuned from 1571.52 to 1539.26 nm with the whole cavity fixed. The Kelly sidebands indicate that the laser stays in a conventional soliton operation within this range. The SWCNT-SA's broadband nonlinear optical performance and polarization robustness facilitate a stable mode-locking state when the laser is tuned. As seen in the purple curve, due to the other transmission peak of the AOI, there is some weaker spectral energy appearing around 1555 nm. This spectral energy even becomes stronger when it is tuned to 1560 nm with driving frequency of 1.064 MHz. As seen from the black dashed curve plotted in Fig. 5(a), the maximum laser gain of the EDF appears near 1560 nm. If we continue to decrease the driving frequency, the two transmission peaks of the AOI have almost the same redshift. The laser gain has rapid attenuation when the wavelength is beyond 1560 nm. Thus, the additional power in the lasing spectrum will gradually disappear. Figure 6(c) shows the laser tuning process with a finer wavelength interval under a smaller frequency interval of 1 kHz. The limitation of the lasing wavelength tuning step is first dependent on the tuning accuracy of the acousto-optical devices. The tuning accuracy of the acousto-optical devices is theoretically limited by the adjustable electrical resolution of the acoustic frequency. However, for the tuning step of the whole laser system, the bandwidth of the tunable device, the gain flatness, operation stability of the laser cavity, and the generated lasing bandwidth have to be also taken into consideration. Thus, the achieved tuning precision of the laser system should be worse than the theoretical tuning step limitation of around 1 pm. Obviously, devices with higher Q factors and narrower filtering bandwidths can achieve a higher tuning precision, but they will seriously widen the pulse width and even prevent soliton operation. Considering that the 3 dB bandwidths of the output laser are over ~1.5 nm at different tuning channels, this step of ~1 nm has been precise enough for the ultrafast laser to traverse all the wavelengths in this tuning range. It is worth noting that stable soliton operation requires a special cavity gain/loss condition that is mainly influenced by the PZT's inherent uneven amplitude-frequency properties. When the driving frequency is changed with the power of the driving signal constant, the vibration amplitude of the PZT cannot keep constant, resulting in a changeable mode-coupling efficiency during tuning processes. The laser cannot maintain a stable

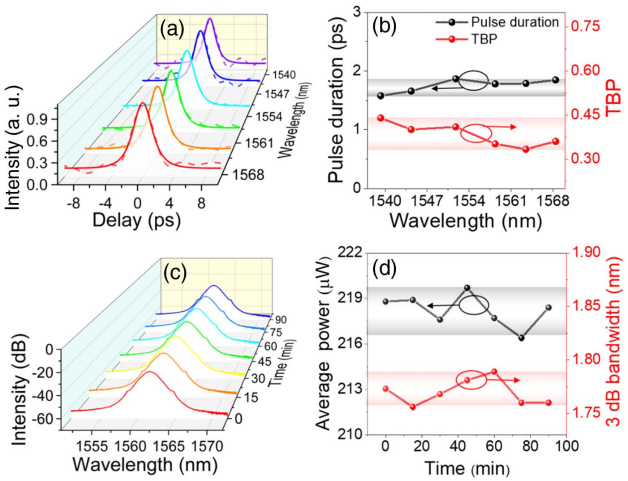

Fig. 7. (a) Autocorrelation trace (dashed line) and the sech^2 fitting curve (solid line) at each wavelength channel; (b) pulse durations and TBPs with variation of the lasing wavelengths; (c) evolution of the output spectrum during a long-term test of the cavity stability for 90 min; (d) fluctuations of the detected average power and 3 dB spectral bandwidth during the long-term test.

mode-locking state when the lasing wavelength is tuned over a certain range. Thus, the tuning range can be further improved by a power pre-calibration of the PZT.

To confirm the maintained ultrafast pulse property if this laser is tuned, autocorrelation traces (dashed line) measured by an autocorrelator (APE, Pulse Check) at different wavelength-tuning channels are also plotted in Fig. 7(a), and all of those experimental traces are well fitted by the sech^2 function (solid line). Both the corresponding pulse durations and TBPs are shown in Fig. 7(b), where the maximum pulse duration is even less than 2 ps. The corresponding TBP just slightly varies from about 0.33 to 0.44, meaning that the near-transform-limited soliton state is sustained at different tuning channels. As shown in Fig. 7(c), to test the long-term cavity stability along with the AOI, both the output spectra and the relative fluctuation of the output average power are monitored for 90 min with the pump power and driving frequency fixed, during which this laser operates in a conventional soliton state, and the spectral shape and center wavelength remain unchanged. The relatively low output power (slope efficiency of ~1%) is due mainly to the output coupling ratio of 10% induced by the OC, the pump power coupling loss in the WDM, and the non-unit quantum efficiency of the 1 m EDF used. Variations of the detected average power and 3 dB spectral bandwidth during this test are shown in Fig. 7(d), where both of the relative power fluctuation and the 3 dB bandwidth variation are less than ±1%, indicating good cavity stability and robustness of this polarization conversion mechanism for ultrafast laser tuning.

5. CONCLUSION

In this work, we have built an acoustically tunable ultrafast EDF laser. The lasing wavelength is tuned by the driving-frequency-dependent AOI, together with the polarization conversion caused by the energy coupling of the core and cladding vector modes. Because of the inner-cavity gain restriction induced by the band-pass spectral property, the lasing wavelength can be tuned over 32 nm by conveniently changing the acoustical wave frequency. Meanwhile, the output maintains near-transform-limited soliton operation with a pulse duration of less than 2 ps, owing to the wideband nonlinear performance of the SWCNT film. This work experimentally demonstrates the superior compatibility between the AOI with the polarization conversion and passively mode-locked mechanism induced by saturable absorption materials, and provides a novel method with easy fabrication to acoustically tune ultrafast lasers in a wide spectral range.

Funding. National Natural Science Foundation of China (NSFC) (61635004, 61705023, 61705024); Key Research and Development Project of Ministry of Science and Technology (2016YFC0801200); Chongqing Postdoctoral Program for Innovative Talents (CQBX201703); Postdoctoral Science Foundation of Chongqing (Xm2017047); Natural Science Foundation of Chongqing (cstc2018jcyjAX0644); Science and Technology on Plasma Physics Laboratory (6142A040 3050817); National Science Fund for Distinguished Young Scholars (61825501).

REFERENCES

1. M. E. Fermann and I. Hart, "Ultrafast fibre lasers," Nat. Photonics **7**, 868–874 (2013).
2. C. Xu and F. W. Wise, "Recent advances in fibre lasers for nonlinear microscopy," Nat. Photonics **7**, 875–882 (2013).
3. W. Fu, L. G. Wright, P. Sidorenko, S. Backus, and F. W. Wise, "Several new directions for ultrafast fiber lasers," Opt. Express **26**, 9432–9463 (2018).
4. U. Keller, "Recent developments in compact ultrafast lasers," Nature **424**, 831–838 (2003).
5. P. Nuernberger, D. Wolpert, H. Weissc, and G. Gerber, "Initiation and control of catalytic surface reactions with shaped femtosecond laser pulses," Phys. Chem. Chem. Phys. **14**, 1185–1199 (2012).
6. H. Zhang, D. Tang, R. J. Knize, L. Zhao, Q. Bao, and K. P. Loh, "Graphene mode locked, wavelength-tunable, dissipative soliton fiber laser," Appl. Phys. Lett. **96**, 111112 (2010).
7. S. Huang, Y. Wang, P. Yan, J. Zhao, H. Li, and R. Lin, "Tunable and switchable multi-wavelength dissipative soliton generation in a graphene oxide mode-locked Yb-doped fiber laser," Opt. Express **22**, 11417–11426 (2014).
8. C. Zhao, Y. Zou, Y. Chen, Z. Wang, S. Lu, H. Zhang, S. Wen, and D. Tang, "Wavelength-tunable picosecond soliton fiber laser with topological insulator: Bi_2Se_3 as a mode locker," Opt. Express **20**, 27888–27895 (2012).
9. A. P. Luo, Z. C. Luo, W. C. Xu, V. V. Dvoyrin, V. M. Mashinsky, and E. M. Dianov, "Tunable and switchable dual-wavelength passively mode-locked Bi-doped all-fiber ring laser based on nonlinear polarization rotation," Laser Phys. Lett. **8**, 601–605 (2011).
10. B. Lu, C. Zou, Q. Huang, Z. Yan, M. AlAraimi, A. Rozhin, and C. Mou, "Wavelength tunable carbon nanotube mode-locked fiber laser based on artificial all-fiber birefringent filter," in *CLEO Pacific Rim* (2018), paper Th1A.4.
11. Z. Sun, D. Popa, T. Hasan, F. Torrisi, F. Wang, E. J. R. Kelleher, J. C. Travers, V. Nicolosi, and A. C. Ferrari, "A Stable, wideband tunable, near transform-limited, graphene-mode-locked, ultrafast laser," Nano Res. **3**, 653–660 (2010).
12. F. Wang, A. G. Rozhin, V. Scardaci, Z. Sun, F. Hennrich, I. H. White, W. I. Milne, and A. C. Ferrari, "Wideband-tuneable, nanotube mode-locked, fibre laser," Nat. Nanotechnol. **3**, 738–742 (2008).

13. D. Li, H. Jussila, Y. Wang, G. Hu, T. Albrow-Owen, R. C. T. Howe, Z. Ren, J. Bai, T. Hasan, and Z. Sun, "Wavelength and pulse duration tunable ultrafast fiber laser modelocked with carbon nanotubes," Sci. Rep. **8**, 2738 (2018).
14. M. Zhang, R. C. T. Howe, R. I. Woodward, E. J. R. Kelleher, F. Torrisi, G. Hu, S. V. Popov, J. R. Taylor, and T. Hasan, "Solution processed MoS_2–PVA composite for subbandgap mode-locking of a wideband tunable ultrafast Er:fiber laser," Nano Res. **8**, 1522–1534 (2015).
15. W. He, M. Pang, and P. St. J. Russell, "Wideband-tunable soliton fiber laser mode-locked at 1.88 GHz by optoacoustic interactions in solid-core PCF," Opt. Express **23**, 24945–24954 (2015).
16. B. Nyushkov, S. Kobtsev, A. Antropov, D. Kolker, and V. Pivtsov, "Femtosecond 78-nm tunable Er:fibre laser based on drop-shaped resonator topology," J. Lightwave Technol. **37**, 1359–1363 (2019).
17. X. Liu and Y. Cui, "Flexible pulse-controlled fiber laser," Sci. Rep. **5**, 9399 (2015).
18. X. He, Z. Liu, and D. N. Wang, "Wavelength-tunable, passively mode-locked fiber laser based on graphene and chirped fiber Bragg grating," Opt. Lett. **37**, 2394–2396 (2012).
19. J. Wang, Y. Yan, A. P. Zhang, B. Wu, Y. Shen, and H. Tam, "Tunable scalar solitons from a polarization maintaining mode-locked fiber laser using carbon nanotube and chirped fiber Bragg grating," Opt. Express **24**, 22387–22394 (2016).
20. S. Li and K. T. Chan, "Electrical wavelength-tunable actively mode-locked fiber ring laser with a linearly chirped fiber Bragg grating," IEEE Photon. Technol. Lett. **10**, 799–801 (1998).
21. J. Wang, M. Yao, C. Hu, A. P. Zhang, Y. Shen, H. Tam, and P. K. A. Wai, "Optofluidic tunable mode-locked fiber laser using a long-period grating integrated microfluidic chip," Opt. Lett. **46**, 1117–1120 (2018).
22. J. Wang, A. P. Zhang, Y. Shen, H. Tam, and P. K. A. Wai, "Optofluidic tunable mode-locked fiber laser using a long-period grating integrated microfluidic chip," Opt. Lett. **40**, 4329–4332 (2015).
23. N. Yan, X. Han, P. Chang, L. Huang, F. Gao, X. Yu, W. Zhang, Z. Zhang, G. Zhang, and J. Xu, "Tunable dual-wavelength fiber laser with unique gain system based on in-fiber acousto-optic Mach–Zehnder interferometer," Opt. Express **25**, 27609–27614 (2017).
24. W. Zhang, L. Huang, F. Gao, F. Bo, G. Zhang, and J. Xu, "Tunable broadband light coupler based on two parallel all-fiber acousto-optic tunable filters," Opt. Express **21**, 16621–16628 (2013).
25. H. S. Park, K. Y. Song, S. H. Yun, and B. Y. Kim, "All-fiber wavelength-tunable acoustooptic switches based on intermodal coupling in fibers," J. Lightwave Technol. **20**, 1864–1868 (2002).
26. H. Zhang, S. Kang, B. Liu, H. Dong, and Y. Miao, "All-fiber acousto-optic tunable bandpass filter based on a lateral offset fiber splicing structure," IEEE Photon. J. **7**, 2700312 (2015).
27. K. J. Lee, D. I. Yeom, and B. Y. Kim, "Narrowband, polarization insensitive all-fiber acousto-optic tunable bandpass filter," Opt. Express **15**, 2987–2992 (2007).
28. W. Zhang, L. Huang, F. Gao, F. Bo, L. Xuan, G. Zhang, and J. Xu, "Tunable add/drop channel coupler based on an acousto-optic tunable filter and a tapered fiber," Opt. Lett. **37**, 1241–1243 (2012).
29. W. Zhang, K. Wei, D. Mao, H. Wang, F. Gao, L. Huang, T. Mei, and J. Zhao, "Generation of femtosecond optical vortex pulse in fiber based on an acoustically induced fiber grating," Opt. Let. **42**, 454–457 (2017).
30. L. Huang, W. Zhang, Y. Li, H. Han, X. Li, P. Chang, F. Gao, G. Zhang, L. Gao, and T. Zhu, "Acousto-optic tunable bandpass filter based on acoustic-flexural-wave-induced fiber birefringence," Opt. Lett. **43**, 5431–5434 (2018).
31. W. Zhang, L. Huang, K. Wei, P. Li, B. Jiang, D. Mao, F. Gao, T. Mei, G. Zhang, and J. Zhao, "Cylindrical vector beam generation in fiber with mode selectivity and wavelength tunability over broadband by acoustic flexural wave," Opt. Express **24**, 10376–10384 (2016).
32. P. Z. Dashti, F. Alhassen, and H. P. Lee, "Observation of orbital angular momentum transfer between acoustic and optical vortices in optical fiber," Phys. Rev. Lett. **96**, 043604 (2006).
33. T. A. Birks, P. St.J. Russell, and D. O. Culverhouse, "The acousto-optic effect in single–mode fiber tapers and couplers," J. Lightwave Technol. **14**, 2519–2529 (1996).
34. H. Jeong, S. Y. Choi, F. Rotermund, K. Lee, and D. Yeom, "All-polarization maintaining passively mode-locked fiber laser using evanescent field interaction with single-walled carbon nanotube saturable absorber," J. Lightwave Technol. **34**, 3510–3514 (2016).
35. Y. Cui and X. Liu, "Graphene and nanotube mode-locked fiber laser emitting dissipative and conventional solitons," Opt. Express **21**, 18969–18974 (2013).
36. Y. Li, L. Gao, W. Huang, C. Gao, M. Liu, W. Huang, and T. Zhu, "All-fiber mode-locked laser via short singlewall carbon nanotubes interacting with evanescent wave in photonic crystal fiber," Opt. Express **24**, 23450–23458 (2016).
37. Y. Song and S. Yamashita, "Carbon nanotube mode lockers with enhanced nonlinearity via evanescent field interaction in D-shaped fibers," Opt. Lett. **32**, 148–150 (2007).
38. X. Han and X. Liu, "Ultracompact fiber laser based on a highly integrated optical device," Photon. Res. **7**, 36–41 (2019).